Mexican Journal of Phytopathology
e-ISSN: 2007-8080

Crossref Open access

Scientific Article

Antifungal activity using ZnO microparticles with different morphologies against *Rhizoctonia* sp.

Flor A. Macías-Mendoza[1,2], Laila Muñoz-Castellanos[1], Juan C. Pantoja-Espinoza[2], Francisco Paraguay-Delgado[2*].
[1]Facultad de Ciencias Químicas, Universidad Autónoma de Chihuahua, Circuito Universitario S/N Campus II, Chihuahua, Chih., CP 31125, México. [2] Centro de Investigación en Materiales Avanzados, S.C. (CIMAV), Av. Miguel de Cervantes #120, Complejo Industrial Chihuahua, Chihuahua, Chih., C.P. 31136, México.

Corresponding Author:
Francisco Paraguay-Delgado
francisco.paraguay@cimav.edu.mx

Section:
Periodical Issue

Received:
August 08, 2025
Accepted:
October 22, 2025
Published:
November 13, 2025
Early Access 2026

Citation:
Macías-Mendoza FA, Muñoz-Castellanos L, Pantoja-Espinoza JC and Paraguay-Delgado F. 2026. Antifungal activity using ZnO microparticles with different morphologies against *Rhizoctonia* sp. Mexican Journal Phytopathology 44(1): 98. https://doi.org/10.18781/R.MEX.FIT.2508-1

ABSTRACT

Background/Objetive. The main objective of the study was to synthesize zinc oxide (ZnO) microparticles (MP) with three types of morphologies (prisms, platelets, and rods) in order to assess their antifungal activity against *Rhizoctonia* sp. It was hypothesized that morphology and concentration were key factors influencing antifungal efficacy. To suggest the potential of customized nanoparticle design in the treatment of fungal diseases.

Materials and Methods. The ZnO MPs were synthesized using the hydrothermal method, designed to obtain three morphologies: prisms, platelets, and rods. They were characterized using scanning electron microscopy (SEM) and X-ray diffraction (XRD). Antifungal activity was evaluated at concentrations of 200, 500, and 1000 ppm against *Rhizoctonia* sp. Statistical analysis was performed using ANOVA and Fisher's LSD test to evaluate the effects of morphology, concentration and time on fungal growth.

Results. At concentrations of 500 and 1000 ppm of MPs, show significant inhibition of *Rhizoctonia* sp. was observed. While at 200 ppm, no significant inhibition was observed compared to the negative control. Sclerotia formation was observed at the lowest concentration in all samples, especially in those with lamellar morphology (ZnO-L) up to 500 ppm. Microscopic evaluation at 200 ppm also revealed structural damage to the hyphae and cytoplasmic condensation. However, this was not observed in the 1000 ppm treatments. Among the different morphologies, ZnO rods (ZnO-R) showed the most effective antifungal activity.

Conclusion. Particles with elongated morphology (rods) showed promising antifungal activity against *Rhizoctonia* sp. The efficacy increased at concentrations of 500 and 1000 ppm, resulting in significant inhibition of fungal growth. The morphology and concentration of the particles are key factors influencing antifungal growth. This result demonstrates that particle morphology plays a crucial role in controlling fungal diseases.

Keywords: Zinc oxide, Pathogenic fungi, Hydrothermal synthesis, SEM, XRD, Mycelial inhibition

INTRODUCTION

The *Rhizoctonia* complex represents a heterogeneous group of filamentous fungi that do not produce asexual spores and share general morphological characteristics, including the formation of mycelium and brown sclerotia (García, 2008). *Rhizoctonia solani*, the most significant species within the genus, affects various crops across families including Poaceae (e.g., corn, rice, wheat, barley, oats), Fabaceae (e.g., soybean, peanut, bean, alfalfa, chickpea, lentil, pea), Solanaceae (e.g., tobacco, potato), Amaranthaceae (e.g., sugar beet), Brassicaceae (e.g., canola), Rubiaceae (e.g., coffee), Malvaceae (e.g., cotton), Asteraceae (e.g., lettuce), Araceae (e.g., pothos), Moraceae (e.g., ficus), and Linaceae (e.g., flax) (Ajayi and Bradley, 2018; DGSV-CNRF, 2020). This pathogen can cause severe damage, resulting in losses of 80 to 100% of seedlings and final yield reductions up to 30%. According to the International Plant Protection Convention (IPPC) and the International Standard for Phytosanitary Measures (ISPM) No. 8, "Determination of Pest Status in an Area," *R. solani* is present throughout areas planted with host crops in México, classifying it as a non-quarantine pest under ISPM No. 5, "Glossary of Phytosanitary Terms" (DGSV-CNRF, 2020).

Various control measures exist for managing pathogens, including certified clean seeds, land tillage, crop rotation to non-host species, seed treatments with fungicides, and, where available, the use of resistant crop varieties (Ajayi and Bradley, 2018). Chemical control through fungicides remains one of the most commonly employed strategies in modern agriculture due to its efficiency, speed, practicality, and economic viability (Jáquez-Matas *et al*., 2022). However, fungal populations targeted by these chemicals can develop resistance over time (Carmona and Sautua, 2017). Additionally, the ability of *R. solani* to overwinter as long-lived sclerotia in the soil and its capacity to infect a wide range of crops make crop rotation alone an insufficient management strategy, highlighting the necessity for alternative control options (Ajayi and Bradley, 2018; Akber *et al*., 2023).

The application of nanotechnology in agriculture is particularly interesting given the mass production of agricultural products required to meet global demand (Mridha, *et al*., 2025). Nanomaterials offer alternatives for improving, mitigating, and remedying collateral problems associated with modern agriculture (Rodríguez and Díaz, 2024).

Among these materials, oxide particles such as ZnO, TiO_2, CuO, Fe_2O_3 are commonly used in various fields (Lira *et al*., 2018; Zhu *et al*., 2019) TiO_2 nanoparticles (NPs) have applications in cosmetics, functional fibers, plastics, inks, paints, fine ceramics, and as food colouring, also serving as protective barriers in consumable packaging (Zhu *et al*., 2019). Ag NPs are valued for their antimicrobial activity and are incorporated into surfaces intended for food contact (Lira *et al*., 2018). CuO NPs are used in superconductors, thermal resistance applications, coating additives, antibacterial materials, and magnetic materials. ZnO NPs, apart from being toxic to human tumor cells, have demonstrated antimicrobial activity, either inhibiting or enhancing microbial growth (Zhu *et al*., 2019).

The antifungal activity of ZnO has been documented against several pathogens. For instance, ZnO particles synthesized via hydrothermal and co-precipitation methods demonstrated antifungal activity against *Colletotrichum gloeosporioides*, inhibiting spore germination and causing hyphal deformation (De la Rosa *et al*., 2018). Against *Erythricium salmonicolor*, the pathogen responsible for the pink disease in coffee, ZnO NPs ranging from 20 to 45 nm exhibited significant antifungal capacity (Arciniegas *et al*., 2017). Moreover, ZnO NPs have shown antifungal activity against *Fusarium oxysporum* by

inhibiting mycelial growth and sporulation *in vitro* (González *et al*., 2021). Similarly, several studies have confirmed the antifungal activity of ZnO particles against *Rhizoctonia solani* (Al-Dhabaan *et al*., 2017; Khan and Siddiqui, 2021; Al-Zaidi *et al*., 2023).

However, Pariona *et al.* (2020) note that few studies have been conducted on the impact of ZnO particle morphology on their antifungal activity. Therefore, the present study aimed to synthesize ZnO microparticles (ZnO MPs) with three distinct morphologies to evaluate their *in vitro* antifungal activity against *Rhizoctonia* sp.

MATHERIALS AND METHODS

Chemicals. The reactives used were agar from the SIGMA ALDRICH brand, denatured ethyl alcohol 96% from the GOLDEN BELL brand, and distilled water. For the antifungal evaluation, PDA agar from the BD BIOXON brand was used, and as a positive control, the fungicide commercially named INTERTHIRAM 480 (ICF), with the active ingredient Thiram (Bis(dimethylthiocarbamoyl) disulphide), with a composition of Thiram 42% by weight, equivalent to 480 g of active ingredient per litre.

Synthesis of ZnO MPs. The hydrothermal synthesis method was carried out to obtain MPs with three distinct three-dimensional morphologies. These shapes were achieved by using zinc acetate as a precursor and varying the concentration of potassium hydroxide. The molar ratio between zinc acetate and potassium hydroxide was 1:9 for rod-shaped ZnO (ZnO-R), 1:3 for lamellar forms (ZnO-L), and 1:1 for hexagonal prisms (ZnO-P). For each synthesis, zinc acetate and potassium hydroxide were simultaneously dissolved in tri-distilled water (15 mL), followed by the dropwise addition of 96% ethanol (15 mL). The resulting solution was then transferred into an autoclave (46 mL) and placed in a muffle furnace at 160 °C for 18 h. After that, the precipitate particles were collected, transferred to 35 mL centrifuge tubes, and then washed twice with distilled water. This process involved centrifugation at 5000 rpm for 5 min, followed by decanting the supernatant each time. Finally, the plastic tubes containing the washed precipitate were placed in an oven at 80 °C for 12 h. After drying, the material was recovered, finely ground in an agate mortar, and weighed.

Characterization of MPs. The physicochemical characterization (size, shape) was conducted using scanning electron microscopy (Jeol JSM-7401F SEM). The structure was studied using X-ray diffraction (XRD) patterns, which were obtained with a Philips X-Pert diffractometer operating at 40 kV and 30 mA, utilizing Cu Kα radiation (λ = 0.15418 nm) in Bragg-Brentano geometry. The scanning angle 20 was between 20 and 80°, with a step size of 0.015°. The patterns were indexed for ZnO, and the JCPDS card # (00-036-1451) was used for reference (Sedefoglu, 2023).

Preparation of cultures poisoned with MPs. The poisoned culture media with ZnO MPs were prepared following the method described by Guerrero *et al*. (2007), with some modifications. Three types of MPs (ZnO-P, ZnO-L, and ZnO-R) were incorporated into the PDA culture medium.

The required amounts of MPs and inoculum concentration factor (ICF) were added to each Petri dish (90 mm diameter), followed by the necessary volume of PDA culture medium to achieve final concentrations of 200 (C), 500 (B), and 1000 (A) ppm. Plates containing only PDA medium were prepared as negative controls. Each concentration was

prepared in triplicate. The culture media were previously held for 24 hours to evaluate their sterility.

Fungal Inoculation. The antifungal activity of ZnO MPs against *Rhizoctonia* sp. was evaluated using the method described by Derbalah *et al*. (2019) with some modifications. A strain of *Rhizoctonia* sp., isolated from a diseased potato acquired in Chihuahua Capital, was used for the assay. For this assay, a total of 39 Petri dishes were prepared: 27 for the ZnO MPs treatments, three independent replicates for the negative control, and nine for the positive control (ICF).

A 5 mm diameter agar disc containing a 7-day-old *Rhizoctonia* sp. culture was placed in each Petri dish, which was then incubated at 27 ± 1 °C for 7 days. Radial growth was measured every 24 h. using a calliper.

Microscopic analysis. After seven days of inoculation, wet mounts were prepared in duplicate. Small portions of the fungus were collected from the replicated Petri dishes and placed on slides with a drop of lactophenol cotton blue stain, covered with a coverslip, and observed under a ZEISS Primostar 1 microscope.

Statistical Analysis. A factorial design with three factors was carried out, whose general model is shown in equation (1):

$$y_{ijkl} = m + MP_i + C_j + D_k + MPi*Cj + MPi*D_k + Cj*D_k + MPi*Cj*D_k + e_{ijkl} \quad (1)$$

Where y_{ijkl} is the response variable (mycelial growth in mm), m is the overall mean, MP_i represents the type of nanoparticle MP with levels ZnO-P, ZnO-R, ZnO-L, and ICF, C_j corresponds to the nanoparticle concentrations at 200, 500, and 1000 ppm, D_k denotes the days of growth monitoring (levels 1 to 7), *l* is the number of replicates, and *e* is the error term. The model also includes two-way interactions ($MP_i * C_j$, $MP_i * D_k$, and $C_j * D_k$) as well as a three-way interaction ($MP_i * C_j * D_k$).

Grubbs and Kolmogorov–Smirnov tests were applied to detect outliers and assess the normality of the data, respectively. Subsequently, an analysis of variance (ANOVA) was performed to identify significant effects of the factors and their interactions. Finally, multiple comparison tests of means were conducted using Fisher's least significant difference (LSD) test. All analyses were carried out using MINITAB 20.3 and OriginPro 2021, with a significance level of $p \leq 0.05$.

RESULTS

Physicochemical characterization. The SEM micrographs for the three morphologies and the size distributions of the MPs are shown in Figure 1. The images for each morphology were included at low and high magnification. Most of them exhibit a hexagonal shape, with varying sizes for each type. The micrographs in Figures 1A and 1D show hexagonal prism particles (ZnO-P) with an average size of 8487 ± 2074 nm, and most of them exhibit marked dips on their surface (Figure 1D). In the case of the lamellar particles (ZnO-L), it can be observed that all of them are in different orientations (Figure 1B and Figure 1E). They have an average diameter of 508 ± 155 nm and show an approximate thickness of 60 nm, forming a smooth surface. In the case of rod-shaped particles (ZnO-R), the images show elongated hexagonal prism particles with a pointed shape (Figure 1C and Figure 1F), and they have

an average length of 2326 ± 1437 nm. These images confirm the three morphological types of particles.

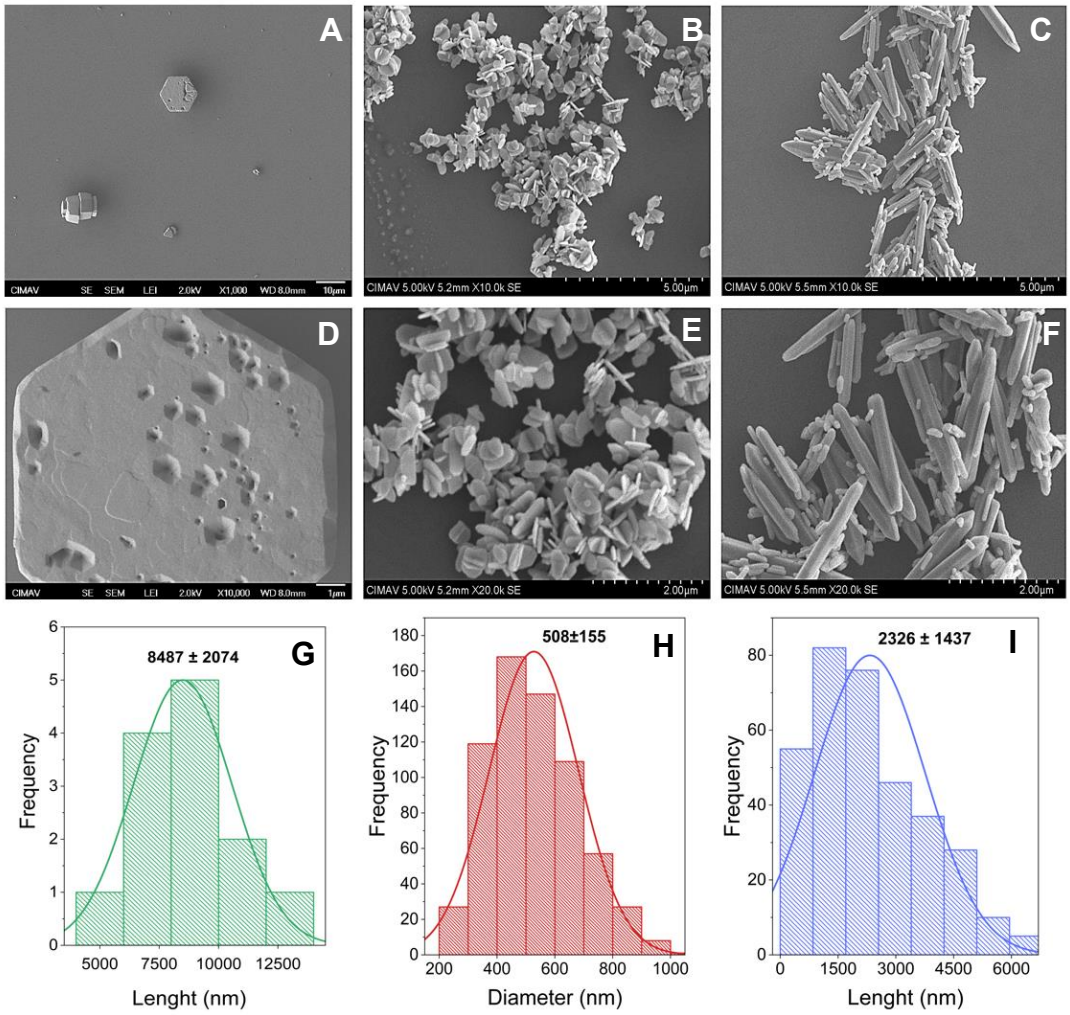

Figure 1. Images of the three morphologies of ZnO particles obtained by SEM, ZnO-P (**A**, **D**), ZnO-L (**B**, **E**), and ZnO-R (**C**, **F**). Size distribution: ZnO-P (**G**), ZnO-L (**H**), and ZnO-R (**I**).

The X-ray diffraction patterns show a similar profile for all obtained samples. Figure 2 shows that all patterns exhibit a polycrystalline structure. As we can see, the intensities do not change proportionally. However, the particles have distinct shapes, as seen in Figure 1. This patterns were indexed for ZnO using the JCPDS card No. 00-036-1451. These results confirm the crystallinity of the obtained particles for three morphologies.

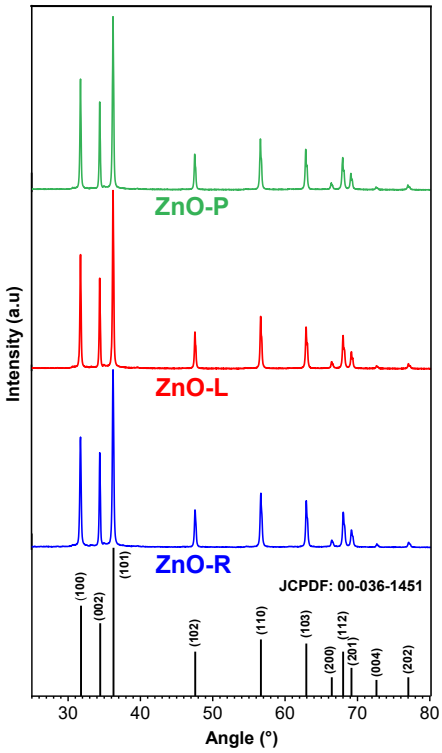

Figure 2. X-ray Diffraction (XRD) patterns of the three zinc oxide samples: ZnO-P (green), ZnO-L (red), and ZnO-R (blue). All diffraction peaks match the hexagonal wurtzite structure of ZnO (reference JCPDF: 00-036-1451).

Antifungal Activity of ZnO MPs Against *Rhizoctonia* sp.

Macroscopic appearance. Figure 3, shows the average growth measurements of *Rhizoctonia* sp. (in mm) over time. The values belong to the mean of three test antifungal replicates, and the error bars represent the standard deviation. On the first day, the negative control exhibited a growth of 13.5 ±0.42 mm. At the lowest concentration (200 ppm), ICF showed an increase of 11.9±0.57 mm. In contrast, for the ZnO-P sample, a growth of 12.6±2.11mm was measured, indicating that the nanoparticle treatments had minimal antifungal activity at this early stage. At the same concentration, the ZnO-L sample exhibited a diameter of 8.9±0.26 mm, and the ZnO-R sample showed an 8.3±0.36 mm diameter.

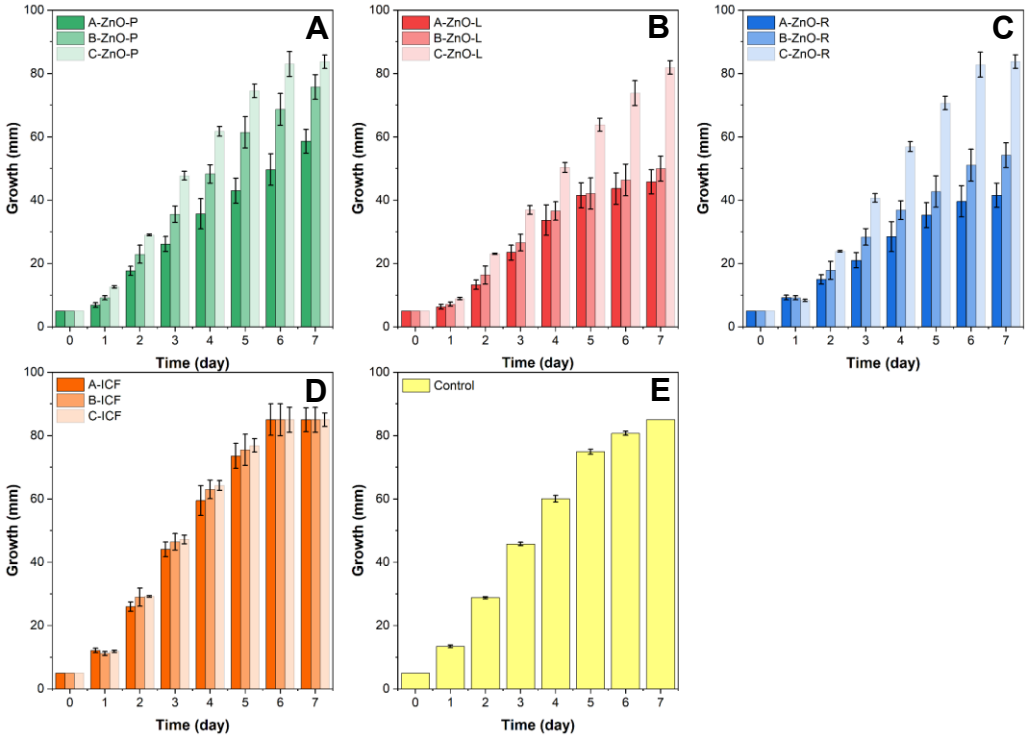

Figure. 3 The growth (mm) of *Rhizoctonia* sp. over time (days) for the samples. (**A**) ZnO-P, (**B**) ZnO-L, (**C**) ZnO-R in comparison to ICF (**D**) and the Negative Control (**E**). The labels (A, B, and C) in the graphics mean A: is at 1000 ppm, B: is at 500 ppm, and C: is at 200 ppm.

After three days of incubation, the negative control reached 45.7±0.52 mm of growth, a value exceeded by both the minimum and medium concentrations of ICF, which recorded 47.2±2.5 mm and 46.4±1.25 mm, respectively. As well as by the minimum concentration of ZnO-P, which reached 47.7±5.05 mm. On the same day, the maximum concentration of ZnO-R displayed the highest antifungal activity, with a growth inhibition of 21±2.36 mm.

On the sixth day, the control exhibited a growth of 80.7±0.64 mm, which was exceeded by all three concentrations of ICF and by the minimum concentrations of ZnO-P and ZnO-R, which showed growths of 83±3.46 mm and 82.7±3.93 mm, respectively. These results highlight the lower antifungal effectiveness of these particular treatments under these conditions.

The inspection using images on the seventh day is presented in Figure 4, further illustrating the differences among treatments. In these images, the numbers (1, 2, and 3) represent the three times of repetition, and the letters A, B, and C denote the 1000, 500, and 200 ppm concentrations, respectively. At the lowest concentration (200 ppm, column C), the nanoparticle treatments did not show a notable difference compared to the negative control (Figure 4E). At the medium concentration (500 ppm, column B), sample ZnO-P (Figure 4A) was the treatment causing the least inhibition—apart from ICF—followed by ZnO-R (Figure 4C). In contrast, ZnO-L (Figure 4B) exhibited the strongest inhibition of *Rhizoctonia* sp. at this concentration. At the highest concentration (1000 ppm, column A), significant inhibition was observed in all treatments, with ZnO-R (Figure 4C) showing the highest antifungal activity, followed by ZnO-L (Figure 4B).

Another important observation was the presence of sclerotia—the resistant structures of *Rhizoctonia* sp.—which were detected in all treatments, including ICF, and a concentration

of 200 ppm. At 500 ppm, only ZnO-P (Figure 4A) exhibited sclerotia, while at 1000 ppm, none of the treatments resulted in their formation.

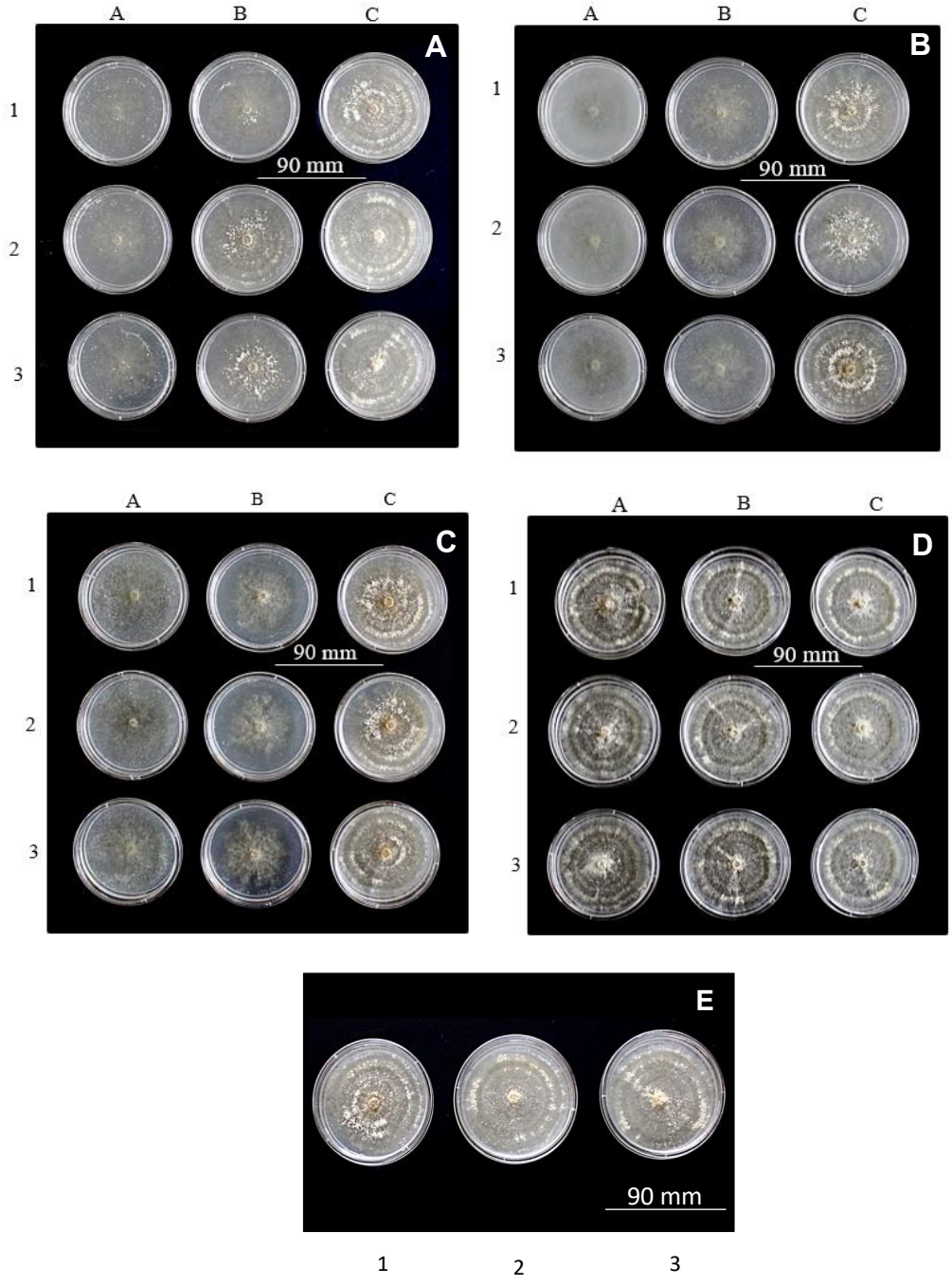

Figure. 4 Macroscopic morphology of aerial mycelium. *Rhizoctonia* sp. on PDA Agar with Nanoparticles – images were acquired at the seventh day inspection, (**A**) ZnO-P, (**B**) ZnO-L, (**C**) ZnO-R in comparison to ICF (**D**), and the Negative Control (**E**). The column labels (A, B, and C) in the graphics represent the following concentrations: A, 1000 ppm; B, 500 ppm; and C, 200 ppm. The numbers labelled 1, 2, and 3 mean the number of repetitions.

Microscopic appearance. Images acquired by the optical microscope are shown in Figure 5. The files A, B, and C belong to 1000, 500, and 200 ppm concentration, respectively. These images revealed long septate hyphae with consistent size in the negative control. The branching of these hyphae was perpendicular, and the tips of the terminal septa appeared slightly curved and narrow.

At the minimum concentration, treatments with ZnO-P and ZnO-L samples, as well as for the ZnO-P sample at the medium concentration and all three concentrations of ICF, exhibited the formation of hyphae resembling synema structures characterized by conidiophores grouped in tufts or brush-like formations (Ormeño, 2024). Additionally, a noticeable loss of plasma membrane integrity was observed, particularly in ZnO-R, where hyphal thickness varied, and in ZnO-L, where coiling of hyphae occurred at the medium concentration.

At the highest concentration (1000 ppm, file A), all treatments resulted in a complete loss of mycelial structure, with varying hyphal thickness, coiled hyphae, and condensation of material believed to be cytoplasm, as observed under the optical microscope (Figure 5).

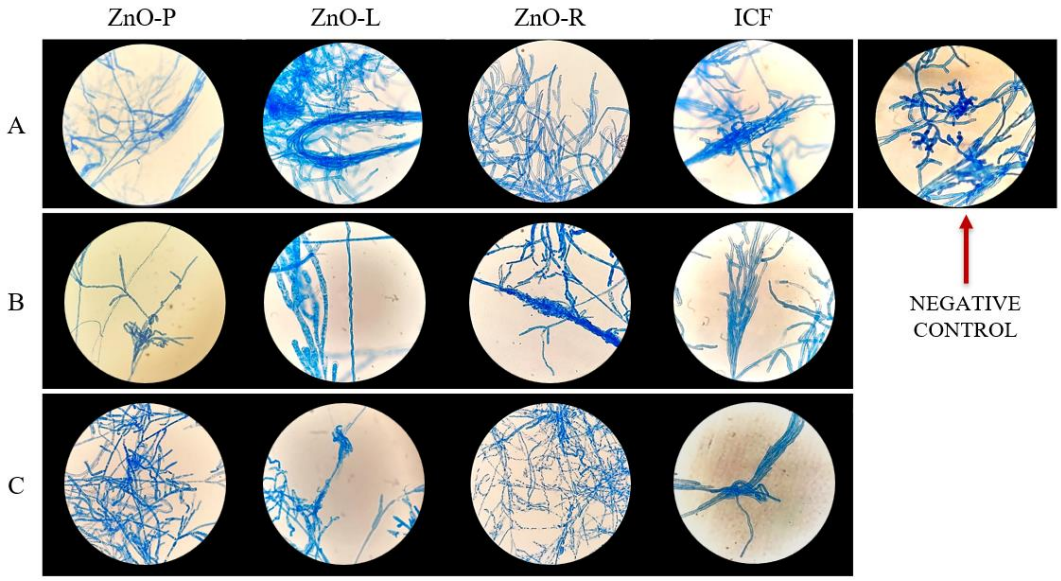

Figure 5. Microscopic Morphology of *Rhizoctonia* sp. on PDA Agar with Concentrations of A: 1000 ppm, B: 500 ppm, and C: 200 ppm of MPs; ZnO-P, ZnO-L, ZnO-R in comparison to ICF and the Negative Control after 7 days of growth. The optical microscope magnification was 40X. Lactophenol Blue.

Statistical Analysis. The results of the data analyses relating to the normality hypothesis are shown in Grubbs' test analysis, which shows the absence of outliers ($p = 0.05$). Similarly, the Kolmogorov-Smirnov test confirmed the normality hypothesis ($p = 0.05$).

The ANOVA summary is presented in Table 1. The F-value of the model was statistically significant ($p < 0.05$), indicating that the linear model was adequate for the analysis. The fitting parameter R^2 value was 0.98, indicating that the model explains a significant amount of variance. Moreover, for all sources of variation, the calculated F-values were markedly higher than the corresponding $F_{Critical}$ values (F-value » $F_{Critical}$), and in all cases the associated p-values were < 0.05. These results demonstrate that the effects observed are statistically significant and reinforce the reliability of the model.

Table 1. ANOVA summary for mycelial growth (mm) as a function of microparticle type, concentration, and incubation days.

Source	DF	SS Adjusted	MS Adjusted	F-value	F_{Critic}	p-value
MP	3	15052	5017.2	502.48	2.66	0.000
Concentration	2	12581	6290.4	630.00	3.05	0.000
Day	6	111770	18628.3	1865.68	2.13	0.000
MP*Concentration	6	4047	674.5	67.55	2.13	0.000
MP*Day	18	3246	180.3	18.06	1.65	0.000
Concentration*Day	12	3337	278.1	27.85	1.74	0.000
MP*Concentration*Day	36	2051	57.0	5.71	1.49	0.000
Error	168	1677	10.0			

DF: degrees of freedom. SS: Sum square. MS: Medium Square. F: Fisher statistics, Calculated and Critical. p: probability.

The ANOVA revealed significant differences in the treatment, concentration, and day factors, as well as in the double and triple interactions regarding the response variable (growth). The results obtained through the ANOVA support the previous observations in Figures 3 and 4.

The comparison of means analysis using Fisher's LSD (Least Significant Difference) test is shown in the Figures 6A, 6B, and 6C, which correspond to the comparisons among treatments, concentrations, and days, respectively. As can be seen, the comparison of means at different levels for both treatment and concentration on the respective days reveals significant differences, as none of the intervals contains a value of 0.

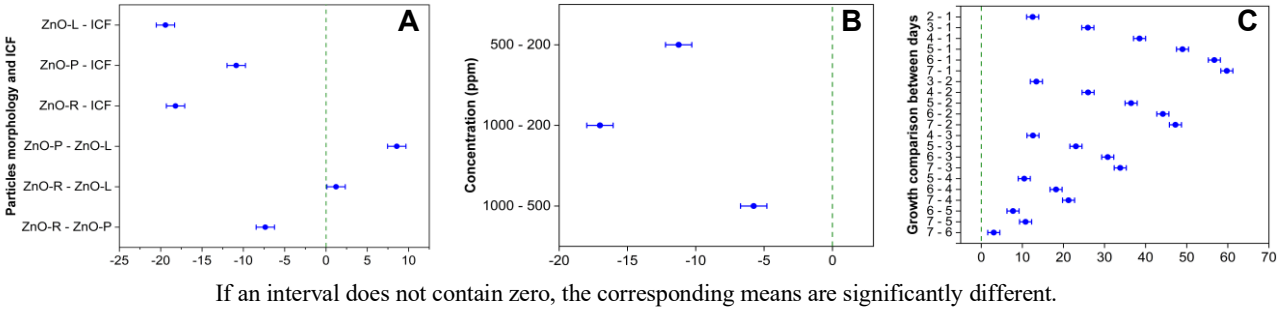

Figure 6. Differences of Means test for Growth (mm) by Fisher´s LSD test comparison of (**A**) treatments, (**B**) concentrations, and (**C**) between days.

DISCUSSION

Although XRD patterns confirm the same crystalline phase in all samples, SEM micrographs reveal significant morphological differences among particles. The observed variations in particle shape and size confirm that the synthesis conditions have a marked influence on morphology (Gulati *et al*., 2016; Moazzen *et al*., 2012; Phan and Nguyen, 2017; Shaba *et al*., 2021).

The macroscopic growth of fungi reveals concentration-dependent antifungal activity of ZnO nanoparticles against *Rhizoctonia* sp. Although minimal inhibition was observed at 200 ppm, particularly for ZnO-P and ICF, the ZnO-L and ZnO-R microparticles showed higher initial suppression of fungal growth at the same concentration. These qualities of the particles suggest that both morphology and surface properties influence their antifungal performance, as reported in previous studies too (Cruz *et al*., 2023; Mantecón, 2015).

The significant decrease in fungal growth observed for the ZnO-R sample at 1000 ppm indicates a particularly strong antifungal effect, which can be attributed to its elongated morphology, providing a larger active surface area and facilitating more effective interactions with fungal cells (Descanse *et al*., 2023). This morphology-dependent behaviour has been well-documented in the literature for ZnO nanostructures, where the shape and size are found to correlate with enhanced antimicrobial efficacy (Tsror, 2010; Mendes *et al*., 2024).

In addition, the absence of sclerotia formation at higher concentrations is highly significant. Sclerotia serve as survival structures for *Rhizoctonia* sp., enabling it to persist under adverse conditions and constituting the primary inoculum for future infections (Tsror, 2010). The suppression of sclerotia at 1000 ppm in all treatments, particularly in ZnO-L and ZnO-R type MPs, suggests that these nanoparticles not only inhibit fungal growth but also interfere with the pathogen life cycle, offering a potential advantage over conventional treatments such as ICF (Mantecón, 2015).

The findings, as revealed by microscopic images, show that ZnO microparticles have a significant morphological effect on *Rhizoctonia* sp. hyphae, with the intensity of this effect increasing at higher concentrations. The presence of synema-like structures in ZnO-P and ZnO-L treatments, as well as in those with ICF, suggests that exposure to these agents may induce morphological adaptations or stress responses in the fungus (Ormeño, 2024).

The observed variability in the thickness and coiling of hyphae, especially with ZnO-R and ZnO-L sample treatments, indicates cell deterioration and could reflect alterations in cell wall growth and cytoskeleton stability, phenomena commonly reported in fungal cells exposed to nanomaterials. These morphology changes are consistent with previous studies describing nanomaterial-induced alterations in fungi growing (Desvani *et al*., 2018; Garrido, 2016).

At the highest concentration, the complete loss of mycelial morphology, along with cytoplasmic condensation, suggests severe cell damage. Such effects may be attributed to oxidative stress mechanisms, in which nanoparticles disrupt cellular organelles and increase the production of reactive oxygen species (ROS) (Fu *et al.,* 2014; León *et al*., 2022). The role of ROS in nanoparticle-induced toxicity is widely documented, as they can cause lipid peroxidation, protein denaturation, and DNA damage, ultimately leading to cell death (Fu *et al*., 2014).

These results highlight the potential of ZnO microparticles, especially at high concentrations, to exert antifungal activity through physical alteration of cellular structures and biochemical mechanisms related to oxidative stress. This dual mode of action could position ZnO microparticles as a promising alternative or a complement to traditional antifungal agents in the management of pathogens such as *Rhizoctonia* sp.

Statistical analyses confirm the reliability of the experimental data and the suitability of employing parametric methods for further evaluation. The absence of outliers and verification of normality by the Kolmogorov-Smirnov test, along with residual plots, provide strong evidence supporting the integrity of the dataset. Such rigorous statistical validation is essential when evaluating biological phenomena, particularly in antifungal assays where variability can be high (Field, 2013).

Significant ANOVA results indicate that the factors of treatment type, concentration, and exposure time (in days) have a strong influence on fungal growth. The high correlation R^2 value (0.98) indicates an excellent fit of the model to the experimental data, suggesting that almost all of the variability in the growth measurements is explained by the

experimental variables and their interactions. These findings are consistent with the trends observed in Figures 3 and 4, which emphasize morphological and growth differences between treatments.

Fisher LSD test further clarifies the specific differences between treatment groups, concentrations, and days, revealing significant differences between all conditions evaluated. The fact that none of the confidence intervals include zero reinforces the conclusion that the treatments had measurable and statistically significant effects on fungal growth. Overall, the statistical results validate the experimental observations and confirm the efficacy of specific ZnO MPs treatments in inhibiting fungal growth, particularly at higher concentrations and with prolonged exposure times. These findings support the potential application of ZnO-R particles as antifungal agents, which justifies future research aimed at exploring their efficacy under different environmental conditions and against other phytopathogenic fungi.

CONCLUSIONS

Particles with different morphologies of ZnO exhibit a significant variation in antifungal activity. When comparing the activity of various morphologies of ZnO particles, it was concluded that none of the morphologies exhibited antifungal activity at the minimum concentration (200 ppm). However, at the medium concentration (500 ppm) and the maximum concentration (1000 ppm), all test nanoparticles exhibited an inhibitory effect, considering both growth and the presence of sclerotia. At the medium concentration, the laminar particles (ZnO-L) yielded the best results. In contrast, at the maximum concentration, the rod-type particles (ZnO-R) proved to be the most effective inhibitors. The effects of MP concentration, day, and their interactions were statistically significant for the growth of *Rhizoctonia* sp. Finding the "p" value less than 0.05.

This result confirms the potential for using particles with different morphologies in agriculture and represents a future possibility for using ZnO particles as fungicides. However, *in vivo* studies would be necessary to verify and visualize the effects of ZnO particles on plants.

Limitations

This study was conducted under *in vitro* conditions, and results may differ in real environments or more complex biological systems. Only one pathogen (*Rhizoctonia* sp.) was evaluated, which limits the generalizability of the findings to other fungal species. Additionally, potential ecotoxicological or phytotoxic effects of the MPs were not assessed, which should be addressed in future studies.

Conflicts interest

The authors declare that they have no conflicts of interest regarding the publication of this article.

Funding

This research received no external funding.

Acknowledgments

The first author would like to thank SECIHTI for its financial support as a research assistant at SNII-III. The authors would like to thank the laboratories at CIMAV, Chihuahua, México, especially Andrés Issak González Jacquez, for his technical assistance in performing X-ray diffraction characterization of the samples used in this research. They also thank the Faculty of Chemical Sciences at the Autonomous University of Chihuahua for providing space for the antifungal evaluation of the ZnO NPs and Yecli Cecilia Varela Lozano for his support with the experimental development.

Author contributions

Flor Macías-Mendoza: Conceptualization, Data curation, Writing – original draft. **Laila Muñoz-Castellaños**: Methodology, Validation, Writing – review & editing. **Juan C. Pantoja-Espinoza**: Formal analysis, Supervision, Visualization, Writing – review & editing. **Francisco Paraguay-Delgado**: Investigation, Project administration, Writing – review & editing.

REFERENCES

Akber MA, Mubeen M, Sohail MA, Khan SW, Solanki MK, *et al*. 2023. Global distribution, traditional and modern detection, diagnostic, and management approaches of *Rhizoctonia solani* associated with legume crops. Frontiers in Microbiology 13:1091288. doi: 10.3389/fmicb.2022.1091288.

Al-Dhabaan F, Shoala T, Ali A, Alaa M and Abd-Elsalam K. 2017. Chemically-produced copper, zinc nanoparticles and chitosan–bimetallic nanocomposites and their antifungal activity against three phytopathogenic fungi. International Journal of Agricultural Technology. 13:753-769. ISSN 1686-9141

Al-Zaidi W, Ali A, and Muhsen T. 2023. Efficacy of nanoparticle zinc oxide in the resistance of fungus *Rhizoctonia solani* causing black scurf disease in local potatoes. Caspian Journal of Environmental Sciences 21:95–103. https://doi.org/10.22124/CJES.2023.6199

Arciniegas P, Patiño M, Mosquera L, Guerrero J and Rodríguez J. 2017. ZnO nanoparticles (ZnO-NPs) and their antifungal activity against coffee fungus *Erythricium salmonicolor.* Applied Nanoscience 7:225–241. https://doi.org/10.1007/s13204-017-0561-3

Ajayi O and Bradley C. 2018. *Rhizoctonia solani:* Taxonomy, population biology and management of *Rhizoctonia* seedling disease of soybean. Plant Pathology 67:3–17. https://doi.org/10.1111/ppa.12733

Carmona M y Sautua F. 2017. La problemática de la resistencia de hongos a fungicidas. causas y efectos en cultivos extensivos. Agronomía & Ambiente 37:1-19. http://agronomiayambiente.agro.uba.ar/index.php/AyA/article/view/60-

Cruz G, Solis R, Ramirez J, Solis J, Gómez M, *et al*. 2023. Actividad de recubrimientos de quitosano, nanopartículas de quitosano y ZnO contra hongos aislados e identificados molecularmente de frutas con potencial de exportación en la zona norte del Perú. Manglar 20:397-403. https://doi.org/10.57188/manglar.2023.046

De la Rosa S, Martínez P, Gomez S, Corral M, Quintana P, *et al*. 2018. Antifungal activity of ZnO and MgO nanomaterials and their mixtures against *Colletotrichum gloeosporioides* strains from tropical fruit. Bioinorganic Chemistry and Applications 2018:3498527. https://doi.org/10.1155/2018/3498527

Derbalah A, Elsharkawy MM, Hamza A and El-Shaer A. 2019. Resistance induction in cucumber and direct antifungal activity of zirconium oxide nanoparticles against *Rhizoctonia solani*. Pesticide Biochemistry and Physiology 157:230–236. https://doi.org/10.1016/j.pestbp.2019.03.018

Descanse J, Betancourth C, Salazar C y Sañudo B. 2023. Estudio epidemiológico de *Rhizoctonia solani* Kühn en cinco genotipos comerciales de papa (*Solanum tuberosum* L.) de Nariño. Revista de Investigación Agraria y Ambiental 14:73-89. https://doi.org/10.22490/21456453.6353

Desvani S, Lestari I, Wibowo H, Supyani N, Poromarto S, *et al*. 2018. Morphological characteristics and virulence of *Rhizoctonia solani* isolates collected from some rice production areas in some districts of Central Java. AIP Conference Proceedings 2011:020068. https://doi.org/10.1063/1.5054472

DGSV-CNRF. 2020. Dirección General de Sanidad Vegetal. Obtenido de: https://www.gob.mx/cms/uploads/attachment/file/600968/Pudrici_n_de_la_ra_z.pdf. Consulta, octubre 2024.

Field A. 2013. Discovering statistics using IBM SPSS statistics. Fourth Edition. Sage Publications Ltd. USA. ISBN:978-1-4462-4918-5. https://scholar.google.com/scholar?hl=en&as_sdt=0%2C5&q=Discovering+statistics+using+IBM+SPSS+statistics&btnG=

Fu P, Xia Q, Hwang H, Ray P and Yu H. 2014. Mechanisms of nanotoxicity: Generation of reactive oxygen species. Journal of Food and Drug Analysis, 22: 64–75. https://doi.org/10.1016/j.jfda.2014.01.005

García M. 2008. Reseña de "Aspectos de sistemática y biología del complejo *Rhizoctonia*". Fitosanidad 12:147-159. https://www.redalyc.org/articulo.oa?id=209115572003

Garrido C. 2016. Evaluación de la actividad micoparasítica de 15 cepas de *Trichoderma* spp. frente a *Rhizoctonia solani,* utilizando frijol caupí (*Vigna unguiculata*) en laboratorio. Tesis, Universidad Nacional de Trujillo. Ciencias Agropecuarias. Trujillo, Perú.

González A, Hernández A, Betancourt R, Ochoa Y, Valdez L, *et al*. 2021. Antifungal activity of zinc oxide nanoparticles in *Fusarium oxysporum- Solanum lycopersicum* pathosystem under controlled conditions. Journal of Phytopathology 169:533–544. https://doi.org/10.1111/jph.13023

Guerrero E, Solís S, Hernández F, Flores A, Sandoval V, *et al*. 2007. Actividad biológica *in vitro* de extractos de *Flourensia cernua* D.C. en Patógenos de Postcosecha: *Alternaria alternata* (Fr.:Fr.) Keissl., *Colletotrichum gloeosporioides* (Penz.) Penz. y Sacc. y *Penicillium digitatum* (Pers.:Fr.) Sacc. Revista Mexicana de Fitopatología 25:48–53. e-ISSN 2007-8080.

Gulati S, Sachdeva M and Bhasin KK. 2018. Capping agents in nanoparticle synthesis: Surfactant and solvent system. AIP conference proceedings 1953:030214. https://doi.org/10.1063/1.5032549

Jáquez-Matas SV, Pérez-Santiago G, Máquez-Linares MA y Pérez-Verdín G. 2022. Impactos económicos y ambientales de los plaguicidas en cultivos de maíz, alfalfa y nogal en Durango, México. Revista Internacional de Contaminación Ambiental. 38:219-233. https://doi.org/10.20937/RICA.54169

Khan M and Siddiqui Z. 2021. Role of zinc oxide nanoparticles in the management of disease complex of beetroot *(Beta vulgaris L.*) caused by *Pectobacterium betavasculorum, Meloidogyne incognita* and *Rhizoctonia solani*. Horticulture, Environment, and Biotechnology 62:225–241. https://doi.org/10.1007/s13580-020-00312-z

León J, Vázquez R and Juarez K. 2022. Desbalance del sistema antioxidante causado por la exposición a nanopartículas de óxido de zinc y óxido de cobre. Mundo Nano Revista Interdisciplinaria En Nanociencia y Nanotecnología 15:1-13. https://doi.org/10.22201/ceiich.24485691e.2022.29.69701

Lira R, Méndez B, Santos G y Vera RI. 2018. Potencial de la nanotecnología en la agricultura. Acta universitaria 28:9–24. https://doi.org/10.15174/au.2018.1575

Mantecón, J. 2015. Fungicidas aplicados al suelo como estrategia de manejo integrado de enfermedades en papa, bajo escenarios de elevada infestación inicial y residual. Revista Latinoamericana de la Papa 19:29-39 https://dialnet.unirioja.es/servlet/articulo?codigo=5512105

Mendes AR, Granadeiro CM, Leite A, Pereira E, Teixeira, *et al*. 2024. Optimizing Antimicrobial Efficacy: Investigating the Impact of Zinc Oxide Nanoparticle Shape and Size. Nanomaterials, 14: 638. https://doi.org/10.3390/nano14070638

Moazzen MA, Borghei SM and Taleshi F. 2012. Change in the morphology of ZnO NPs upon changing the reactant concentration. Applied Nanoscience 3:295–302. https://doi.org/10.1007/s13204-012-0147-z

Mridha D, Lamsal B and Antonangelo JA. 2025. Nanotechnology in agriculture: Innovations for sustainability and greenhouse gas mitigation-A review. Science of the Total Environment, 995:180065. https://doi.org/10.1016/j.scitotenv.2025.180065

Ormeño, S. 2024. Introducción a los Hongos Fitopatógenos. E.T.S.I. en Topografía, Geodesia y Cartografía (UPM). Primera Edición. Madrid, España. 218p. Archivo Digital UPM. https://oa.upm.es/82782/

Pariona N, Paraguay-Delgado F, Basurto-Cereceda S, Morales-Mendoza JE, Hermida-Montero LA, *et al*. 2020. Shape-dependent antifungal activity of ZnO particles against phytopathogenic fungi. Applied Nanoscience 10: 435-443. https://doi.org/10.1007/s13204-019-01127-w

Phan CM and Nguyen HM. 2017. Role of Capping Agent in Wet Synthesis of Nanoparticles. The Journal of Physical Chemistry A 121:3213–3219. https://doi.org/10.1021/acs.jpca.7b02186

Rodríguez V and Díaz E. 2024. Potencial de los nanomateriales en la agricultura: retos y oportunidades. Mundo Nano 17:1-20. https://doi.org/10.22201/ceiich.24485691e.2024.32.69802

Sedefoglu N. 2023. Characterization and photocatalytic activity of ZnO nanoparticles by green synthesis method. Optik, 288: 171217. https://doi.org/10.1016/j.ijleo.2023.171217

Shaba EY, Jacob JO, Tijani JO and Suleiman MA. 2021. A critical review of synthesis parameters affecting the properties of zinc oxide nanoparticle and its application in wastewater treatment. Applied Water Science 11:1-48. https://doi.org/10.1007/s13201-021-01370-z

Tsror, L. 2010. Biology, epidemiology and management of *Rhizoctonia solani* on potato. Journal of Phytopathology 158:649–658. https://doi.org/10.1111/j.1439-0434.2010.01671.x

Zhu Y, Wu J, Chen M, Liu X, Xiong Y, *et al*. 2019. Recent advances in the biotoxicity of metal oxide nanoparticles: Impacts on plants, animals and microorganisms. Chemosphere 237:124403. https://doi.org/10.1016/j.chemosphere.2019.124403